Defect-Engineered Magnetic Field Dependent Optoelectronics of Vanadium Doped Tungsten Diselenide Monolayers

Katharina Nisi, Jonas Kiemle, Lukas Powalla, Alessio Scavuzzo, Tuan Dung Nguyen, Takashi Taniguchi, Kenji Watanabe, Dinh Loc Duong, Marko Burghard,* Alexander W. Holleitner,* and Christoph Kastl*

The ability to dope transition metal dichalcogenides such as tungsten diselenide (WSe$_2$) with magnetic transition metal atoms in a controlled manner has motivated intense research with the aim of generating dilute magnetic semiconductors. In this work, semiconducting WSe$_2$ monolayers, substitutionally doped with vanadium atoms, are investigated using low-temperature luminescence and optoelectronic spectroscopy. V-dopants lead to a p-type doping character and an impurity-related emission ≈160 meV below the neutral exciton, both of which scale with the nominal percentage of V-dopants. Measurements using field-effect devices of 0.3% V-doped WSe$_2$ demonstrate bipolar carrier tunability. The doped monolayers display a clear magnetic hysteresis in transport measurements both under illumination and without illumination, whereas the valley polarization of the excitons reveals a nonlinear *g*-factor without a magnetic hysteresis within the experimental uncertainty. Hence, this work on V-doped WSe$_2$ provides crucial insights concerning suitable characterization methods on magnetic properties of doped 2D materials.

1. Introduction

Monolayer semiconducting transition metal dichalcogenides (TMDCs) of group IV transition metals, such as MoS$_2$, WS$_2$, and WSe$_2$, exhibit direct band gaps in the visible range and a weak dielectric screening, with the latter significantly enhancing the Coulomb interaction leading to emergent exciton physics up to room temperature.[1] Due to the inherently reduced screening, the material properties become increasingly susceptible to lattice defects in the atomically thin limit. State of the art growth methods and encapsulation protocols have focused on reducing unwanted defects to reveal the intrinsic limit of optical and electronic properties.[2,3] The emergent field of defect engineering, however, aims at intentionally introducing defects in 2D semiconductors, not only to control basic electronic and optical properties, but also to implement advanced functionality, such as chemical sensing, catalytic activity, quantum light emission, or magnetic order.[4–7]

A growing interest has focused on magnetic doping of 2D semiconductors, with the aim of creating dilute magnetic semiconductors. Generally, their bandwidth reduction and larger band gaps make 2D materials favorable for itinerant magnetic order with high Curie-Néel temperatures.[8] Additionally, the intrinsically strong spin-orbit coupling provides an interesting platform for (opto)spintronics.[9,10] A natural choice for (magnetic) dopants are other transition metals, since they incorporate easily into the metal sublattice.[11–14]

K. Nisi, J. Kiemle, A. W. Holleitner, C. Kastl
Walter Schottky Institut and Physics Department
Technical University of Munich
85748 Garching, Germany
E-mail: holleitner@wsi.tum.de; christoph.kastl@wsi.tum.de

K. Nisi, J. Kiemle, A. W. Holleitner, C. Kastl
Munich Center for Quantum Science and Technology (MCQST)
80799 Munich, Germany

L. Powalla, A. Scavuzzo, M. Burghard
Max-Planck-Institut für Festkörperforschung
70569 Stuttgart, Germany
E-mail: m.burghard@fkf.mpg.de

The ORCID identification number(s) for the author(s) of this article can be found under https://doi.org/10.1002/adom.202102711.

T. D. Nguyen, D. L. Duong
Center for Integrated Nanostructure Physics (CINAP)
Institute for Basic Science (IBS)
Suwon 16419, Republic of Korea

T. D. Nguyen, D. L. Duong
Department of Energy Science
Sungkyunkwan University
Suwon 16419, Republic of Korea

T. Taniguchi
International Center for Materials Nanoarchitectonics
National Institute for Materials Science
Tsukuba 305-0044, Japan

K. Watanabe
Research Center for Functional Materials
National Institute for Materials Science
Tsukuba 305-0044, Japan

Calculations for TMDC monolayers, such as MoS_2 and WS_2, suggest that doping with manganese, nickel, niobium, tantalum or vanadium can induce ferromagnetic order with Curie temperatures up to 170 K.[8,15,16] Among different host materials, monolayer WSe_2 is deemed especially suitable due to its good ambipolar gate tunability and larger spin-orbit splitting compared to the Mo-based TMDCs, which can be beneficial for stabilizing the magnetic order.[13,17–21] Furthermore, (doped) WSe_2 bulk crystals can be grown at low defect densities, enabling proof-of-concept devices, but also high quality wafer-scale monolayers can be grown by metal organic chemical vapor deposition (CVD), ensuring scalability and applicability.[2,13,22]

In vanadium-doped WSe_2, theoretical and experimental works have provided first evidence for a room temperature, long-range, (ferro)magnetic order.[18,20,23,24] Vanadium incorporates into the tungsten lattice with negligible strain, as verified by atomic resolution imaging, and, in line with theoretical predictions, it results in an acceptor state close to the valence band, as demonstrated by tunneling spectroscopy and the p-type of field-effect devices.[12,13,17,23–27] For dilute atomic concentrations between 0.1% and 4%, signatures of magnetic order were obtained in CVD-grown V-WSe_2 monolayers via magnetic force imaging up to room temperature and magnetic hysteresis loops at low-temperature.[23,24] Further studies found a hysteretic magnetoresistance up to room temperature, a remnant behaviour of the low-temperature resistance in (zero-)field cooling experiments, as well as signatures of finite excitonic valley polarization in room temperature photoluminescence (PL).[17,26,28] As the underlying mechanism, a hybridization of the vanadium acceptor states with the valence band of WSe_2 was proposed enabling an efficient RKKY-interaction between the localized (bound) spin states on the vanadium atoms and the itinerant (free) carriers.[19,29] Lastly, theory predicts that the magnetic exchange is turned off for a large, electrostatically induced electron doping due to a complete filling of vanadium defect states.[19] This requires carrier densities of 1.6×10^{13} cm^{-2} for vanadium concentrations of 1.6%.

Here, we explore magnetic ordering in V-doped WSe_2 by magnetooptic and optoelectronic measurements. Specifically, we study the low-temperature PL spectra of WSe_2 grown by chemical vapour transport (CVT) capped/encapsulated with hexagonal boron nitride (hBN) for three different vanadium concentrations (0.3%, 0.5% and 1%, given in atomic percent) and compare it to undoped WSe_2.[17] Vanadium doping leads to a p-type character of the monolayers as evidenced by a dominating emission from positively charged trions with increasing dopant concentration. Furthermore, we observe an impurity-induced emission, which is likely related to recombination of a bound exciton via the vanadium defect states and is stable up to 200 K. Gate-dependent PL demonstrates a good charge tunability and preserved semiconducting character of WSe_2 at moderate vanadium concentration (0.3%). Magnetic field-dependent charge transport exhibits a clear hysteresis for p-type conduction, whereas photocurrent measurements reveal hysteresis throughout the whole gateable range. Concurrently, we find indications of a non-linear exciton g-factor in magneto-PL. Our results highlight the potential of substitutional doping to engineer magnetic properties of 2D TMDCs.

2. Results

Bulk crystals of V-doped WSe_2 were grown by CVT (see Section 4). All concentrations of V-dopants (atomic percent) are the nominal amounts added during the CVT-process. For low doping concentrations (on the order of few atom percent), vanadium is substitutionally incorporated into the tungsten lattice of WSe_2 (**Figure 1**a) and results in p-type doping with vanadium acceptor states near the valence band.[12,19,22–24,26] For the investigated crystal batch, the substitutional incorporation was independently confirmed by Raman measurements (Figure 1b), where we find a small, but systematic blue shift of the overlapping E^1_{2g} and A_{1g} mode for monolayer WSe_2 with increasing doping concentration (inset of Figure 1b). The shift may either arise from a decrease of the average unit cell mass or from a carrier density dependence of the Raman modes, as reported for example in gated monolayer MoS_2.[30] Specifically for WSe_2, a similar blue shift of the E^1_{2g} and 2LA(M) modes has been observed upon plasma-induced p-type doping.[31–33] Importantly, Raman signatures of VSe_2 are absent and spatial mapping shows no indications of possible VSe_2 clustering. We note that defect activated modes, which have previously been reported for V-doped WSe_2 prepared by metal organic CVD, are not detectable.[13] This may be a consequence of the different growth methods, as in the present study monolayers are exfoliated from bulk, CVT-grown WSe_2, eliminating substrate-related strain, which is often prevalent for direct CVD growth onto oxide substrates.[34]

Figure 1c shows PL spectra of monolayer WSe_2 for different nominal doping concentrations, which are 0% (pristine), 0.3%, 0.5% and 1%. All samples are fully encapsulated in hBN, with the exception of the capped 0.3% V-doped sample (for details see Figure S1, Supporting Information). All spectra were taken at low-temperature ($T = 1.7$ K), and they are referenced to the neutral exciton to aid comparison between the different samples. The excitation wavelength was 637 nm (1.946 eV). Pristine WSe_2 typically exhibits slight n-type character due to unintentional doping from intrinsic defects, and therefore we assign the peaks to a neutral exciton (X_0), a negative trion (X^-), and a negatively charged biexciton (XX^-).[35,36] Due to inhomogeneous broadening, it is not possible to resolve independently singlet and triplet trion. The red-shift of the trion (29 meV) and the biexciton (48 meV) relative to the neutral exciton agree with reported values.[37] Consistently, the excitation power dependences are linear for the neutral exciton ($\alpha = 1$), close to linear for the trion ($\alpha = 1.2$), but super-linear ($\alpha = 1.5$) for the biexciton (see Figures S2 and S3, Supporting Information).[38,39]

Upon increasing the vanadium concentration, the overall PL is strongly quenched in accordance with previous reports on doped WS_2 and WSe_2.[13,40] Furthermore, a broad emission band arises about 160 meV below the neutral exciton. The relative intensity of this emission band increases monotonously with doping concentration (Figure 1d), suggesting that it stems from transitions involving vanadium defects. More precisely, we interpret the V-related emission as a consequence of a hole dopant level near the valence band of WSe_2, where bound exciton transitions involve the delocalized WSe_2 conduction band and the localized vanadium defect level. We note that the additional broadening of the excitonic features observed in the
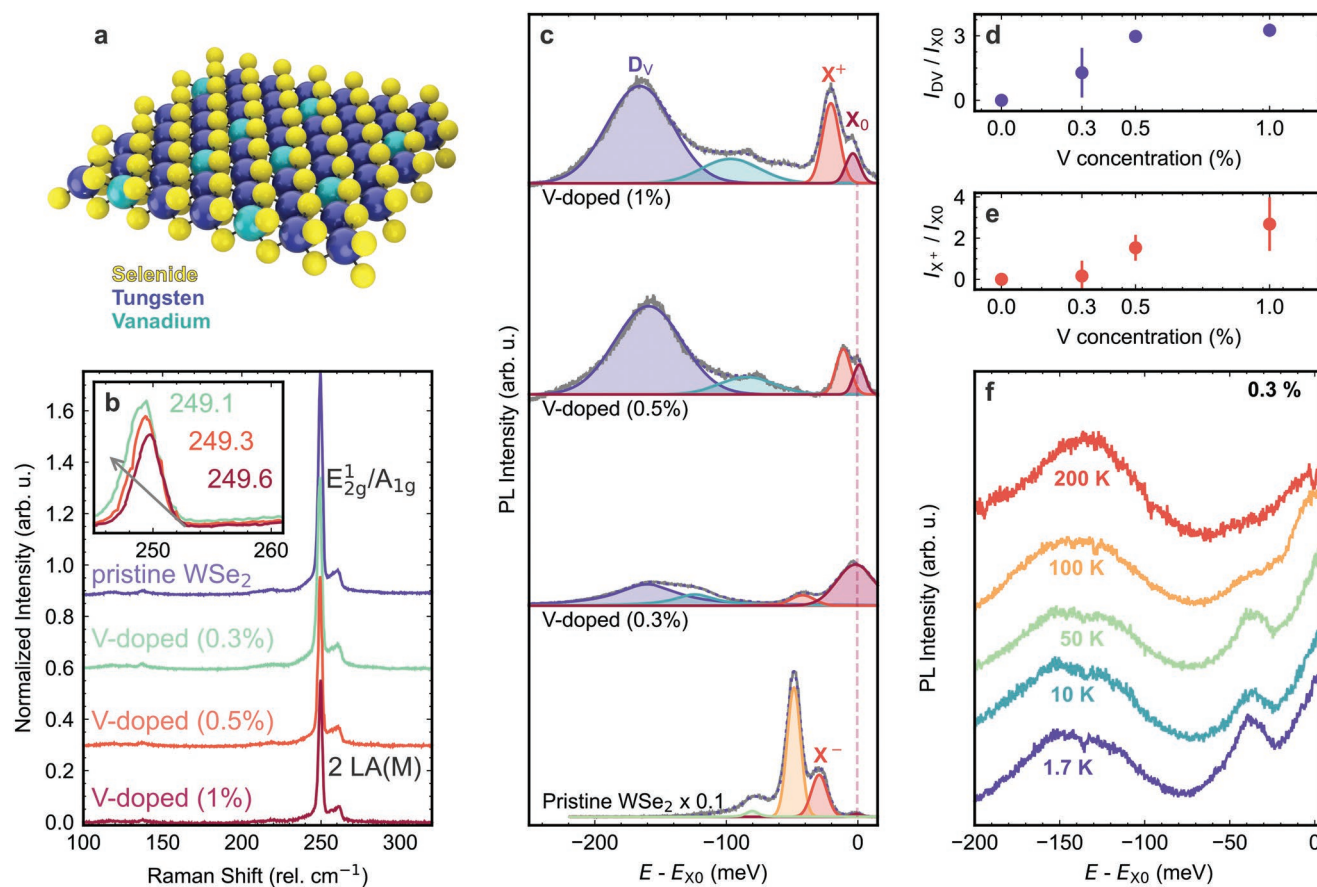
Figure 1. Optical spectra of V-doped monolayer WSe_2. a) Schematic crystal structure. b) Normalized Raman spectra showing the overlapping E^1_{2g} and A_{1g} (249 cm^{-1}) and 2LA(M) (262 cm^{-1}) modes. The inset demonstrates a sub-wavenumber shift of 0.8 cm^{-1} per 1% V-dopants. c) Low-temperature PL spectra of monolayer V-WSe_2 ($T = 1.7$ K, 637 nm, $P_{laser} = 1$ mW). The emission energies are referenced to the neutral exciton. Pristine (undoped) WSe_2 exhibits a neutral exciton X_0 and a negative trion X^- redshifted by 29 meV. At high excitation density, a third peak (yellow) consistent with a negatively charged biexciton XX^- is observed 48 meV below X_0. The intensity of the pristine sample was scaled by 0.1. Vanadium doping results in p-type character with a positive trion emission X^+ redshifted by 17 meV. D_V is a defect emission due the vanadium dopant levels. d) Integrated intensity of D_V versus intensity of X_0 as function of V-concentration. e) Intensity ratio between neutral exciton and positive trion as function of concentration. f) Temperature dependent PL at 0.3% vanadium concentration.

0.3% V-doped sample may arise due to the absence of a bottom hBN encapsulation layer. The PL spectra for all three doping concentrations show a second sub-gap emission 85–95 meV below the neutral exciton (light blue peak in Figure 1c). In this energy range, intra- and intervalley dark excitons and their phonon replicas have been reported in undoped WSe_2.[41,42] Emission from such dark transitions typically requires a scattering process, which can be mediated by phonons or lattice defects, such as potentially the vanadium impurities in the doped samples.[43,44] However, a definite assignment of the transitions in this energy range would require samples with reduced inhomogeneous broadening. Vanadium doping of WSe_2 is known to change the carrier doping character from n-type to p-type, and consistently, emission from the negatively charged biexciton decreases and emission from a positively charged trion appears with increasing vanadium content (Figures 1c and 1e).[12,22–24,26] Intriguingly, the defect emission D_V is stable up to 200 K, similar to PL reported on rhenium doped WSe_2.[45] The stability at temperatures above 200 K is notably high compared to localized emitters in 2D transition

metal dichalcogenides, which are often stable only well below 100 K (Figure 1f).[46–48]

In the next step, we characterize the carrier density dependence of the excitonic properties at doping of nominally 0.3%. On the one hand, previous reports evidenced ferromagnetic order at these moderate vanadium concentrations for CVD-grown films.[18,19,23,24,26] On the other hand, the initial PL measurements for 0.3% in Figure 1 indicate a low background carrier density, which is desirable to maintain good tunability. For fabricating the field-effect devices (**Figure 2**a), the 0.3% doped monolayers were exfoliated onto Si/SiO₂ with 300 nm oxide thickness, contacted by Ti/Au electrodes using e-beam lithography and capped by hBN (in the following referred to as sample 1 and 2).

Individual PL spectra at three selected gate voltages are shown for a monolayer device with 0.3% doping in Figure 2b (sample 1). The spectra show the neutral exciton (indicated by the dot), the negatively charged trion (indicated by the triangle) and vanadium defect peak (indicated by the diamond). Figure 2c depicts the integrated areas for the different emission
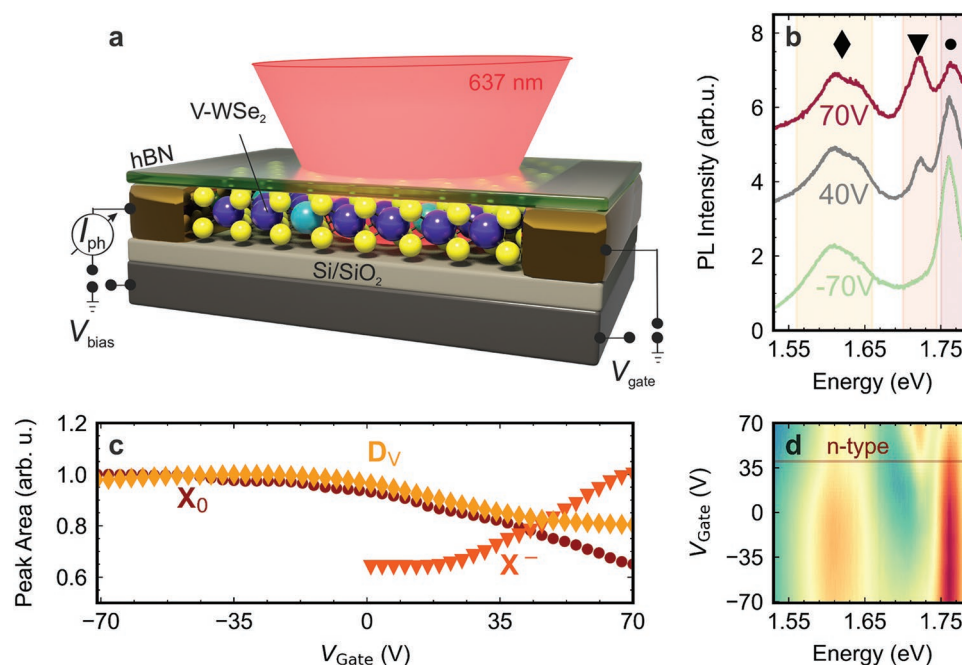
Figure 2. Gate-dependent PL of V-doped WSe_2. a) Schematic of V-doped WSe_2 (0.3%) on a 300 nm Si/SiO_2-substrate with top layer hBN. The TMDC ML is contacted using two gold contacts. b) PL spectra at selected gate voltages for the sketched device with a nominal V-doping of 0.3%. c) Normalized intensities of exciton, trion and impurity emission as function of gate voltage. The intensities are integrated across the spectral ranges indicated in (b). d) This device exhibits compensated character.

peaks defined in Figure 2b as a function of the gate voltage. As expected, the negatively charged trion weight decreases with decreasing gate voltage, that is, when moving toward intrinsic doping.[49] We note that the intensity of the neutral exciton and the vanadium defect appear to be directly correlated, similar to observations on defect emitters due to sulfur vacancies in MoS_2.[50] Based on the trion intensity, the transition from the intrinsic to n-type regime occurs approximately at 40 V (Figure 2d). Therefore, a concentration of 0.3% constitutes an intermediate case, in which the p-type vanadium doping partially compensates the slight intrinsic n-type character.

Having established the carrier tunability of the V-WSe_2 monolayer, we now turn to the magnetic field dependent transport properties. For electrical characterization, the V-WSe_2 layers were contacted in a two-terminal configuration using gold electrodes as sketched in Figure 2a. The transfer curve of sample 2 at 4 V bias is displayed in **Figure 3**a. The dark current exhibits overall low values of a few hundred picoamperes, but a clear tunability from p-type to n-type behavior. The overall good gate tunability at low doping levels agrees with previous studies on substitutionally doped WSe_2, both with rhenium and vanadium dopants.[13,19,23] To improve the signal to noise ratio, we employed differential conductivity measurements at a DC bias of $V_{SD} = 4$ V, a superimposed AC bias $V_{SD} = 0.1$ V, and lock-in detection at 777 Hz. The corresponding hysteresis loops are displayed in Figures 3b–d at gate voltages of –70 V, 0 V and 65 V, respectively. At negative gate voltages (–70 V), the Fermi level is close to the vanadium impurity band, where theory predicts the maximum magnetization.[19] Consistently, a clear hysteresis is observed when the magnetic field is swept from 3 T to –3 T and back. The open triangles highlight the switching

of the hysteresis features close to 0.75 T. At 0 V gate voltage, the Fermi level is deep inside the gap of V-WSe_2, and no dark current is detected within the resolution of our measurements. At large positive gate voltages (+65 V), corresponding to n-type doping, we do not observe a clear hysteresis within the noise level, which may be an indication of the theoretically predicted gate tunability of the magnetization.[19]

The transistor devices fabricated from V-WSe_2 still suffer from high contact resistances, which render detailed electrical characterization difficult.[51–53] To further enhance the sensitivity
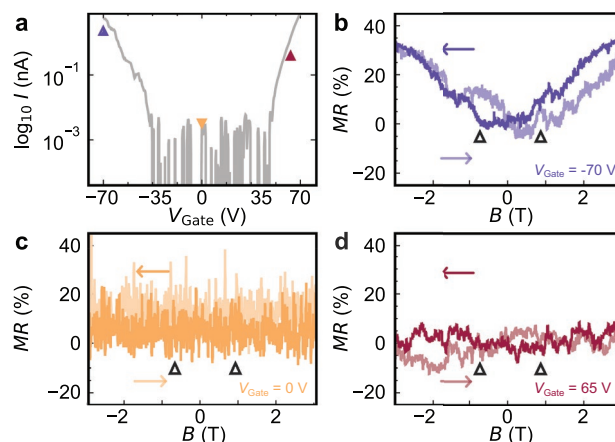

Figure 3. Magneto-transport of V-doped WSe_2. a) Transfer characteristics of the source-drain dark current at 4 V bias voltage (sample 2). b,c,d) Magnetoresistance (MR) (without illumination, $V_{SD} = 4$ V, $dV = 0.1$ V). MR was calculated as following: MR(%) = [R (resistance) – R_0 (resistance at 0 T)]/R_0.
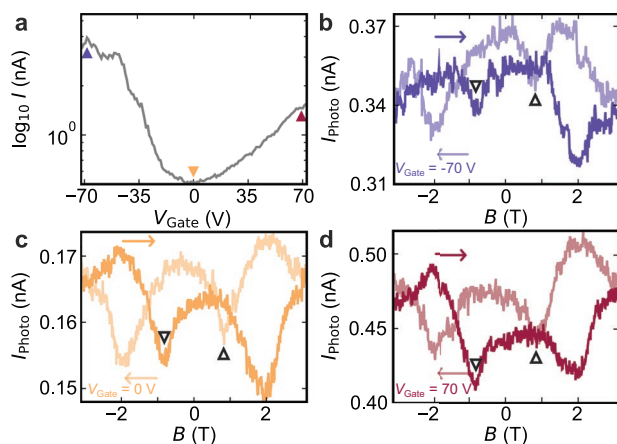
Figure 4. Magneto-photocurrent of V-doped WSe₂. a) Transfer characteristics of the source-drain current under illumination (637 nm) at 2 V bias voltage (sample 1). b,c,d) Magnetic hysteresis loops of the photocurrent. A clear difference between the up-sweep (dark) and down-sweep (light) direction is observed across the full gate voltage regime, b) −70 V, c) 0 V and d) 70 V, respectively.

of our electronic measurements, we illuminated the device with $E_{photon} = 1.95$ eV and $P_{laser} = 0.3$ mW. Furthermore, the illumination allows to establish a close correspondence between the PL and electric transport properties under equivalent experimental conditions. **Figure 4**a depicts the transfer curve of a V-WSe₂ transistor device (0.3%, sample 1). The device scheme is the same as sketched in Figure 2a.

The device exhibits a minimum in photoresponse around $V_{Gate} = 0$ V, which agrees with the intrinsic regime in PL (Figure 2) and transport (Figure 3). Figures 4b–d show magnetic hysteresis loops for the photocurrent measured with circularly polarized light and an excitation wavelength of 637 nm (1.946 eV). The photocurrents at gate voltages −70 V, 0 V and 70 V show a clear magnetic hysteresis with switching features at approximately 2 T and 0.75 T (again highlighted by open triangles), when the magnetic field is swept from 3 T to −3 T and back. A similar magnetic hysteresis has been observed in the dark current of multilayer V-WSe₂, and importantly it was absent in undoped control samples.[17] Since the magnetic hysteresis persists across the full gate range, it is distinct to recent results on multilayer WSe₂, where a hysteresis was only found when the Fermi level was aligned to the in-gap vacancy states.[54]

The B-field and gate-dependence for left circularly polarized light (σ^-) exhibits the exact same behaviour suggesting that the observed hysteresis is independent of the valley polarization of the optically injected carriers. The hysteresis of the photocurrent was reproduced on a second sample (sample 2, Figure S4, Supporting Information) and also for an excitation energy of 1.59 eV, which corresponds to a (near) resonant excitation of the vanadium defect transitions. The fact that the hysteresis is clearly observed throughout the full gate range, in contrast to the dark current measurements in Figure 3, suggests that under illumination the quasi Fermi levels of the photoexcited electrons and holes need to be taken into account, in particular the photoexcitation of the vacancy impurity level.

We further investigate the magnetic behavior by means of magneto-PL measurements of the exciton g-factors from −6 T

to 6 T. **Figure 5**a shows PL spectra of 0.3% V-doped WSe₂ for three different gate voltages (sample 1). Since the inhomogeneous line width broadening (≈15 meV) is considerably larger than the Zeeman shift (≈2 meV), we determined the g-factors from numerical fits of the data as the difference in the peak position between circularly left and circularly right excitation and detection $\Delta E = E_{\sigma^{++}} - E_{\sigma^{--}}$. To avoid over-parametrization of our fit model in the spectral region where the defect-related peaks (purple and blue curve) are not clearly separated, we fixed their energetic separation in the analysis, and we quote a common g-factor for this spectral range.

At −70 V (Figure 5b), the g-factor exhibits a linear magnetic field dependence throughout the applied field range. The determined g-factor for the neutral exciton ($g = -3.3$) is close to the expected value of −4, which is based on the magnetization of the bands in a single particle picture, and it is consistent with experimental values reported for undoped WSe₂.[37,55,56] Since the negatively charged trion is suppressed at −70 V, we could not resolve the Zeeman-shift for this transition. For the vanadium defect transition, we find $g = -2.9$, which can tentatively be explained by transitions between localized defect levels without contributions from the valence band. The latter are expected to yield larger g-factors.[57] The undoped WSe₂ control sample also demonstrates linear g-factors ($g = -4.7$ for the exciton, and $g = -6.4$ for the trion) in line with literature values.

Upon increasing the electron doping via sweeping the gate voltage to 0 V and 70 V, respectively (Figures 5c and 5d), we observe a pronounced nonlinearity of the Zeeman-shift. Similar nonlinear shifts have also been observed for WSe₂ by Wang et al. and for MoS₂ by Klein et al. We can describe the curves with an effective g-factor $\Delta E = g_{eff} \cdot \mu_B \cdot H^* \cdot \tanh(H/H^*)$ according to the model used in ref. [58]. Here, H is the external magnetic field, H^* is a critical magnetic field which phenomenologically describes the nonlinear behavior and μ_B is the Bohr magneton 5.788×10^{-5} eV/T. From this fit model, we assign an effective g-factor (labelled g_{eff}) which corresponds to the slope of the nonlinear curve around $B = 0$ T. Intriguingly, a saturation behavior occurs at magnetic field values of roughly 3 T, which corresponds to the field values in which the hysteresis closes in Figure 4b–d. The nonlinearity is further accompanied by an increased splitting energy and consequently increased effective g-factor for the vanadium defect and trion. The observed nonlinear g-factor and the magnetic hysteresis in Figure 4 are possible signatures of a magnetic order in V-doped WSe₂ samples. Nevertheless, a magnetic hysteresis of the Zeeman shift is not observed within our experimental uncertainty, and the photocurrent hysteresis is independent of the excitation polarization. In addition, nonlinear Zeeman shifts of the exciton have also been reported in pristine WSe₂ and MoS₂.[58,59] The nonlinearity of the g-factor in pristine samples has been assigned to many-body interactions of the exciton with free carriers, although a recent study suggests that also the magnetic moment from intrinsic selenium defects may be relevant.[54]

3. Conclusion

In summary, we report on the magnetooptical and optoelectronic properties of vanadium-doped WSe₂ monolayers. We
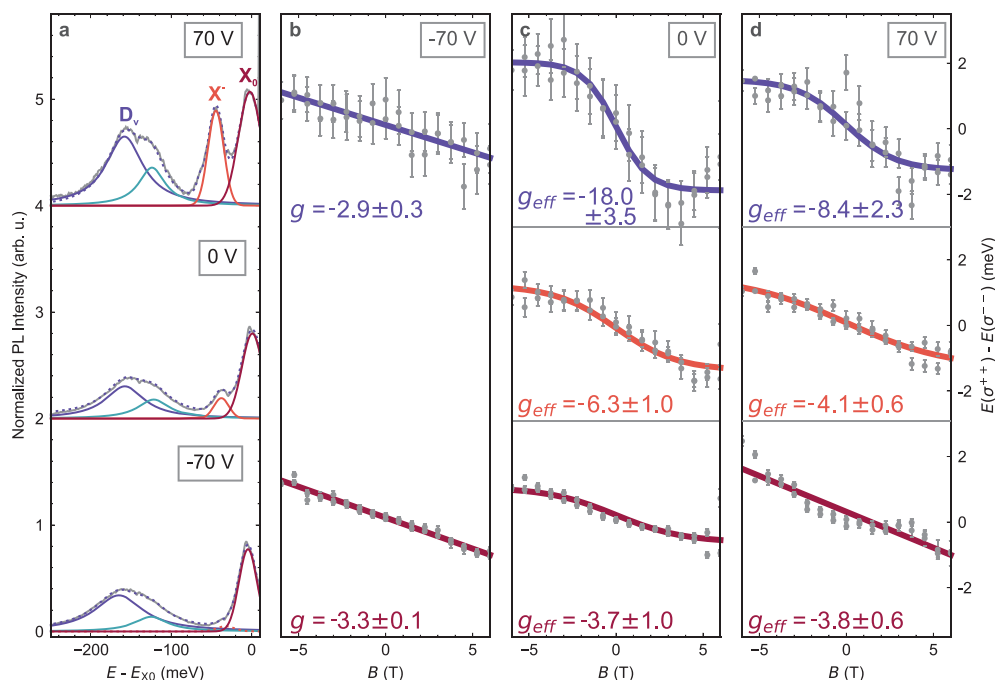
ADVANCED
SCIENCE NEWS

www.advancedsciencenews.com

ADVANCED
OPTICAL
MATERIALS

www.advopticalmat.de

Figure 5. B-field-dependent PL of 0.3% V-doped monolayer WSe$_2$. a) Circularly polarized (σ^{++}) PL spectra of 0.3% V-doped WSe$_2$ at 0 T and +70 V, 0 V, and −70 V. The spectra are fitted with two Lorentzian and two Gaussian for the neutral exciton, negatively charged trion and the two defects, respectively. The difference of the determined peak energies of both configurations, σ^{++} and σ^-, is calculated and fit using a nonlinear fit approach.[58] The resulting energy differences and fits are plotted in panels b–d) for X$_0$, X$^-$ and D$_V$ for each gate voltage, respectively. For −70 V, the emission of X$^-$ is suppressed and no Zeeman shift is resolved. Experimental data in grey, fit in solid lines. A linear dependency is observed for small magnetic fields and a nonlinearity for higher magnetic fields.

find that the incorporation of vanadium into the tungsten lattice leads to a broad emission band 160 meV below X$_0$ from bound excitons and systematic emergence of charged trion emission due to the p-type doping. We provide magnetic field-dependent transport and optoelectronic measurements of 0.3% V-doped WSe$_2$, which show hysteresis within the applied external magnetic field range. Furthermore, we establish good gate tunability of the lightly doped films while maintaining a magnetic hysteresis for different carrier densities. Since the magnetic hysteresis persists across the full gate range, it is distinct to recent results on multilayer WSe$_2$, where a magnetic hysteresis was found only when the Fermi level was aligned to the in-gap vacancy states.[54] In magneto-PL, we find a nonlinear Zeeman shift of the exciton at large n-type doping, but no systematic magnetic field hysteresis. For further studies of the magnetic properties, it will be beneficial to improve the electronic contact characteristics, for example by using metals which form small contact barriers, as has been reported for molybdenum or niobium.[22] By improving the excitonic line widths, for example, by full encapsulation in high quality hBN and by using graphite gate electrodes, the impact of the doping induced magnetic order, which is clearly apparent in electronic transport, may be resolved also for the excitonic ensemble. With optimized devices, local probes, such as photocurrent or Kerr rotation imaging, can potentially be used to elucidate the magnetic structure in more detail. Furthermore, comparison of the effect of in- and out-of-plane magnetic field may shed light on the orientation of the magnetic axes. Lastly, nanoscale magnetometry using nitrogen-vacancy centers in diamond may

allow for a higher magnetic field sensitivity with nanoscale spatial resolution to directly resolve the magnetic ordering in these devices.[60–63] Overall, WSe$_2$ exhibits a rich and complex interplay of charge doping, magnetic doping, defect properties and exciton physics calling for further investigation.

4. Experimental Section

Sample Preparation: Bulk crystals of pristine WSe$_2$ and V-doped WSe$_2$ were grown using a chemical vapor transport (CVT)-growth mechanism with tungsten, selenide and vanadium powder precursors and iodine gas as the transport agent, as reported in ref. [17]. The bulk crystals were exfoliated using mechanical cleavage. Monolayers were transferred onto Si/SiO$_2$ with 300 nm oxide thickness, contacted by Ti/Au electrodes using e-beam lithography and capped by hBN.

PL Measurements: PL was measured at 1.7 K (unless explicitly noted otherwise) in a closed-cycle cryostat with an optional magnetic field up to 6 T in Faraday geometry using a confocal dip-stick microscope. For excitation, a 637 nm diode laser was used with σ^+ or σ^- polarization. The polarization was adjusted using an achromatic $\lambda/4$-waveplate inserted into the beam path. The emission was collected using an achromatic, low-temperature objective (NA = 0.82). The collected light passed through the achromatic $\lambda/4$-waveplate and the polarization was selected by a $\lambda/2$-waveplate and a polarizer inserted into the detection path. The spectrum was analyzed using a 500 mm spectrograph (grating 300 g/mm) and a N$_2$-cooled CCD.

Dark Current Measurements: Transport measurements of 0.3% V-doped WSe$_2$ were investigated at 1.7 K. The gate voltages were applied to the silicon backgate using a sourcemeter, the bias voltages were applied to the source contact, and the current was measured at the drain contact using a transimpedance amplifier simultaneously. The

differential conductance modulated at 777 Hz was measured using a lock-in amplifier with an AC bias amplitude of 0.1 V that was added to a DC bias voltage of 4 V.

Photocurrent Measurements: Optoelectronic properties of 0.3% V-doped WSe_2 were investigated at 1.7 K using the same setup as for PL. The gate voltages were applied to the silicon backgate using a sourcemeter, the bias voltages were applied to the source contact, and the current was measured at the drain contact using a transimpedance amplifier. The excitation wavelength was $\lambda_{exc} = 637$ nm, unless explicitly stated otherwise. The laser intensity was modulated with a modulation frequency of 37 Hz at a 50% duty cycle square-wave and the resulting photocurrent was measured using a lock-in amplifier.

Raman Spectroscopy: Raman spectroscopy of pristine and V-doped WSe_2 were implemented with a 532 nm excitation laser ($P_{laser} = 0.1$ mW) coupled into a commercial confocal microscope (WITec Alpha 300 R) using a 63x (0.7 NA) objective and a 1800 g/mm grating. The spectra were oversampled by moving the grating in sub-cm^{-1} steps. All measurements were conducted at room temperature and in a vacuum chamber (base pressure $<1 \times 10^{-5}$ mbar).

Supporting Information

Supporting Information is available from the Wiley Online Library or from the author.

Conflict of Interest

The authors declare no conflict of interest.

Data Availability Statement

The data that support the findings of this study are available from the corresponding author upon reasonable request.

[1] U. Wurstbauer, B. Miller, E. Parzinger, A. W. Holleitner, *J. Phys. D* **2017**, *50*, 173001.
[2] D. Edelberg, D. Rhodes, A. Kerelsky, B. Kim, J. Wang, A. Zangiabadi, C. Kim, A. Abhinandan, J. Ardelean, M. Scully, D. Scullion, L. Embon, R. Zu, E. J. Santos, L. Balicas, C. Marianetti, K. Barmak, X. Zhu, J. Hone, A. N. Pasupathy, *Nano Lett.* **2019**, *19*, 4371.
[3] J. Wierzbowski, J. Klein, F. Sigger, C. Straubinger, M. Kremser, T. Taniguchi, K. Watanabe, U. Wurstbauer, A. W. Holleitner, M. Kaniber, K. Müller, J. J. Finley, *Sci. Rep.* **2017**, *7*, 12383.
[4] Z. Lin, B. R. Carvalho, E. Kahn, R. Lv, R. Rao, H. Terrones, M. A. Pimenta, M. Terrones, *2D Mater.* **2016**, *3*, 022002.
[5] K. Barthelmi, J. Klein, A. Hötger, L. Sigl, F. Sigger, E. Mitterreiter, S. Rey, S. Gyger, M. Lorke, M. Florian, F. Jahnke, T. Taniguchi, K. Watanabe, V. Zwiller, K. D. Jöns, U. Wurstbauer, C. Kastl, A. Weber-Bargioni, J. J. Finley, K. Müller, A. W. Holleitner, *Appl. Phys. Lett.* **2020**, *117*, 070501.
[6] Q. Liang, Q. Zhang, X. Zhao, M. Liu, A. T. Wee, *ACS Nano* **2021**, *15*, 2165.
[7] J. A. Robinson, B. Schuler, *Appl. Phys. Lett.* **2021**, *119*, 140501.
[8] Y. Gao, N. Ganguli, P. J. Kelly, *Phys. Rev. B* **2019**, *100*, 235440.
[9] E. C. Ahn, *npj 2D Mater. Appl.* **2020**, *4*, 17.
[10] A. Avsar, H. Ochoa, F. Guinea, B. Zyilmaz, B. J. Van Wees, I. J. Vera-Marun, *Rev. Mod. Phys.* **2020**, *92*, 021003.
[11] B. Schuler, J. H. Lee, C. Kastl, K. A. Cochrane, C. T. Chen, S. Refaely-Abramson, S. Yuan, E. Van Veen, R. Roldán, N. J. Borys, R. J. Koch, S. Aloni, A. M. Schwartzberg, D. F. Ogletree, J. B. Neaton, A. Weber-Bargioni, *ACS Nano* **2019**, *13*, 10520.
[12] P. Mallet, F. Chiapello, H. Okuno, H. Boukari, M. Jamet, J. Y. Veuillen, *Phys. Rev. Lett.* **2020**, *125*, 036802.
[13] A. Kozhakhmetov, S. Stolz, A. M. Z. Tan, R. Pendurthi, S. Bachu, F. Turker, N. Alem, J. Kachian, S. Das, R. G. Hennig, O. Gröning, B. Schuler, J. A. Robinson, *Adv. Funct. Mater.* **2021**, *2105252*, 2105252.
[14] L. Loh, Z. Zhang, M. Bosman, G. Eda, *Nano Res.* **2021**, *14*, 1668.
[15] A. Ramasubramaniam, D. Naveh, *Phys. Rev. B* **2013**, *87*, 195201.
[16] M. Luo, S. Y. Hao, Y. T. Ling, *AIP Adv.* **2016**, *6*, 085112.
[17] J. Jiang, L. A. T. Nguyen, T. D. Nguyen, D. H. Luong, D. Y. Kim, Y. Jin, P. Kim, D. L. Duong, Y. H. Lee, *Phys. Rev. B* **2021**, *103*, 014441.
[18] D. L. Duong, S. J. Yun, Y. Kim, S. G. Kim, Y. H. Lee, *Appl. Phys. Lett.* **2019**, *115*, 242406.
[19] D. L. Duong, S. G. Kim, Y. H. Lee, *AIP Adv.* **2020**, *10*, 065220.
[20] S. Tiwari, M. L. Van de Put, B. Sorée, W. G. Vandenberghe, *npj 2D Mater. Appl.* **2021**, *5*, 54.
[21] M. Luo, E. Xu Yu, X. Zhang Qiu, *AIP Adv.* **2018**, *8*, 085212.
[22] A. Klein, P. Dolatzoglou, M. Lux-Steiner, E. Bucher, *Sol. Energy Mater Sol. Cells* **1997**, *46*, 175.
[23] S. J. Yun, D. L. Duong, D. M. Ha, K. Singh, T. L. Phan, W. Choi, Y. M. Kim, Y. H. Lee, *Adv. Sci.* **2020**, *7*, 1903076.
[24] Y. T. H. Pham, M. Liu, V. O. Jimenez, Z. Yu, V. Kalappattil, F. Zhang, K. Wang, T. Williams, M. Terrones, M. H. Phan, *Adv. Mater.* **2020**, *32*, 2003607.
[25] S. Fan, S. J. Yun, W. J. Yu, Y. H. Lee, *Adv. Sci.* **2020**, *7*, 1902751.
[26] B. Song, S. J. Yun, J. Jiang, J. Avila, K. Beach, W. Choi, Y. M. Kim, D. Yoon, H. Terrones, Y. J. Song, M. C. Asensio, D. L. Duong, Y. H. Lee, *Phys. Rev. B* **2021**, *103*, 94432.
[27] S. Li, J. Hong, B. Gao, Y. C. Lin, H. E. Lim, X. Lu, J. Wu, S. Liu, Y. Tateyama, Y. Sakuma, K. Tsukagoshi, K. Suenaga, T. Taniguchi, *Adv. Sci.* **2021**, *8*, 2004438.
[28] L.-A. T. Nguyen, K. P. Dhakal, Y. Lee, W. Choi, T. D. Nguyen, C. Hong, D. H. Luong, Y.-M. Kim, J. Kim, M. Lee, T. Choi, A. J. Heinrich, J.-H. Kim, D. Lee, D. L. Duong, Y. H. Lee, *ACS Nano* **2021**, *15*, 20267.
[29] D. Mastrogiuseppe, N. Sandler, S. E. Ulloa, *Phys. Rev. B* **2014**, *90*, 161403.

[30] B. Miller, E. Parzinger, A. Vernickel, A. W. Holleitner, U. Wurstbauer, *Appl. Phys. Lett.* **2015**, *106*, 122103.

[31] C.-S. Pang, T. Y. Hung, A. Khosravi, R. Addou, Q. Wang, M. J. Kim, R. M. Wallace, Z. Chen, *Adv. Electron. Mater.* **2020**, *6*, 1901304.

[32] S. B. Desai, G. Seol, J. S. Kang, H. Fang, C. Battaglia, R. Kapadia, J. W. Ager, J. Guo, A. Javey, *Nano Lett.* **2014**, *14*, 4592.

[33] A. Khosravi, R. Addou, C. M. Smyth, R. Yue, C. R. Cormier, J. Kim, C. L. Hinkle, R. M. Wallace, *APL Mater.* **2018**, *6*, 026603.

[34] B. Liu, M. Fathi, L. Chen, A. Abbas, Y. Ma, C. Zhou, *ACS Nano* **2015**, *9*, 6119.

[35] A. A. Mitioglu, P. Plochocka, G. Del Aguila, P. C. Christianen, G. Deligeorgis, S. Anghel, L. Kulyuk, D. K. Maude, *Nano Lett.* **2015**, *15*, 4387.

[36] S. H. El-Mahalawy, B. L. Evans, *Phys. Status Solidi B* **1977**, *79*, 713.

[37] Z. Li, T. Wang, Z. Lu, C. Jin, Y. Chen, Y. Meng, Z. Lian, T. Taniguchi, K. Watanabe, S. Zhang, D. Smirnov, S. F. Shi, *Nat. Commun.* **2018**, *9*, 3719.

[38] M. Barbone, A. R. Montblanch, D. M. Kara, C. Palacios-Berraquero, A. R. Cadore, D. De Fazio, B. Pingault, E. Mostaani, H. Li, B. Chen, K. Watanabe, T. Taniguchi, S. Tongay, G. Wang, A. C. Ferrari, M. Atatüre, *Nat. Commun.* **2018**, *9*, 3721.

[39] T. P. Lyons, S. Dufferwiel, M. Brooks, F. Withers, T. Taniguchi, K. Watanabe, K. S. Novoselov, G. Burkard, A. I. Tartakovskii, *Nat. Commun.* **2019**, *10*, 2330.

[40] F. Zhang, B. Zheng, A. Sebastian, D. H. Olson, M. Liu, K. Fujisawa, Y. T. H. Pham, V. O. Jimenez, V. Kalappattil, L. Miao, T. Zhang, R. Pendurthi, Y. Lei, A. L. Elías, Y. Wang, N. Alem, P. E. Hopkins, S. Das, V. H. Crespi, M. H. Phan, M. Terrones, *Adv. Sci.* **2020**, *7*, 2001174.

[41] E. Liu, J. Van Baren, C. T. Liang, T. Taniguchi, K. Watanabe, N. M. Gabor, Y. C. Chang, C. H. Lui, *Phys. Rev. Lett.* **2020**, *124*, 196802.

[42] Z. Li, T. Wang, C. Jin, Z. Lu, Z. Lian, Y. Meng, M. Blei, S. Gao, T. Taniguchi, K. Watanabe, T. Ren, S. Tongay, L. Yang, D. Smirnov, T. Cao, S. F. Shi, *Nat. Commun.* **2019**, *10*, 2469.

[43] M. He, P. Rivera, D. Van Tuan, N. P. Wilson, M. Yang, T. Taniguchi, K. Watanabe, J. Yan, D. G. Mandrus, H. Yu, H. Dery, W. Yao, X. Xu, *Nat. Commun.* **2020**, *11*, 618.

[44] Z. Li, T. Wang, Z. Lu, M. Khatoniar, Z. Lian, Y. Meng, M. Blei, T. Taniguchi, K. Watanabe, S. A. McGill, S. Tongay, V. M. Menon, D. Smirnov, S. F. Shi, *Nano Lett.* **2019**, *19*, 6886.

[45] L. Loh, Y. Chen, J. Wang, X. Yin, C. S. Tang, Q. Zhang, K. Watanabe, T. Taniguchi, A. T. Wee, M. Bosman, S. Y. Quek, G. Eda, *Nano Lett.* **2021**, *21*, 5293.

[46] J. Klein, M. Lorke, M. Florian, F. Sigger, L. Sigl, S. Rey, J. Wierzbowski, J. Cerne, K. Müller, E. Mitterreiter, P. Zimmermann, T. Taniguchi, K. Watanabe, U. Wurstbauer, M. Kaniber, M. Knap, R. Schmidt, J. J. Finley, A. W. Holleitner, *Nat. Commun.* **2019**, *10*, 2755.

[47] P. Tonndorf, R. Schmidt, R. Schneider, J. Kern, M. Buscema, G. A. Steele, A. Castellanos-Gomez, H. S. J. van der Zant, S. Michaelis de Vasconcellos, R. Bratschitsch, *Optica* **2015**, *2*, 347.

[48] E. Liu, J. van Baren, T. Taniguchi, K. Watanabe, Y.-C. Chang, C. H. Lui, *Phys. Rev. Res.* **2019**, *1*, 32007.

[49] E. Liu, J. Van Baren, Z. Lu, M. M. Altaiary, T. Taniguchi, K. Watanabe, D. Smirnov, C. H. Lui, *Phys. Rev. Lett.* **2019**, *123*, 27401.

[50] A. Hötger, J. Klein, K. Barthelmi, L. Sigl, F. Sigger, W. Männer, S. Gyger, M. Florian, M. Lorke, F. Jahnke, T. Taniguchi, K. Watanabe, K. D. Jöns, U. Wurstbauer, C. Kastl, K. Müller, J. J. Finley, A. W. Holleitner, *Nano Lett.* **2021**, *21*, 1040.

[51] K. Sotthewes, R. Van Bremen, E. Dollekamp, T. Boulogne, K. Nowakowski, D. Kas, H. J. Zandvliet, P. Bampoulis, *J. Phys. Chem. C* **2019**, *123*, 5411.

[52] A. Allain, J. Kang, K. Banerjee, A. Kis, *Nat. Mater.* **2015**, *14*, 1195.

[53] D. S. Schulman, A. J. Arnold, S. Das, *Chem. Soc. Rev.* **2018**, *47*, 3037.

[54] T. D. Nguyen, J. Jiang, B. Song, M. D. Tran, W. Choi, J. H. Kim, Y.-M. Kim, D. L. Duong, Y. H. Lee, *Adv. Sci.* **2021**, *8*, 2102911.

[55] J. Förste, N. V. Tepliakov, S. Y. Kruchinin, J. Lindlau, V. Funk, M. Förg, K. Watanabe, T. Taniguchi, A. S. Baimuratov, A. Högele, *Nat. Commun.* **2020**, *11*, 4539.

[56] A. V. Stier, N. P. Wilson, K. A. Velizhanin, J. Kono, X. Xu, S. A. Crooker, *Phys. Rev. Lett.* **2018**, *120*, 057405.

[57] E. Mitterreiter, B. Schuler, A. Micevic, D. Hernangómez-Pérez, K. Barthelmi, K. A. Cochrane, J. Kiemle, F. Sigger, J. Klein, E. Wong, E. S. Barnard, K. Watanabe, T. Taniguchi, M. Lorke, F. Jahnke, J. J. Finley, A. M. Schwartzberg, D. Y. Qiu, S. Refaely-Abramson, A. W. Holleitner, A. Weber-Bargioni, C. Kastl, *Nat. Commun.* **2021**, *12*, 3822.

[58] Z. Wang, K. F. Mak, J. Shan, *Phys. Rev. Lett.* **2018**, *120*, 66402.

[59] J. Klein, A. Hötger, M. Florian, A. Steinhoff, A. Delhomme, T. Taniguchi, K. Watanabe, F. Jahnke, A. W. Holleitner, M. Potemski, C. Faugeras, J. J. Finley, A. V. Stier, *Phys. Rev. Res.* **2021**, *3*, L022009.

[60] A. Kuwahata, T. Kitaizumi, K. Saichi, T. Sato, R. Igarashi, T. Ohshima, Y. Masuyama, T. Iwasaki, M. Hatano, F. Jelezko, M. Kusakabe, T. Yatsui, M. Sekino, *Sci. Rep.* **2020**, *10*, 2483.

[61] J. H. Loubser, J. A. Van Wyk, *Rep. Prog. Phys.* **1978**, *41*, 1201.

[62] F. Jelezko, J. Wrachtrup, *Phys. Status Solidi A* **2006**, *203*, 3207.

[63] M. W. Doherty, N. B. Manson, P. Delaney, F. Jelezko, J. Wrachtrup, L. C. Hollenberg, *Phys. Rep.* **2013**, *528*, 1.

2102711 (8 of 8)